Imaging micro-well detectors for X-ray and gamma-ray applications

J. K. Black, P. Deines-Jones, S. D. Hunter, K. Jahoda

NASA/Goddard Space Flight Center
Laboratory for High Energy Astrophysics
Greenbelt, MD 20771

J. Huang, T. N. Jackson, H. Klauk, W. Qian

Pennsylvania State University
Department of Electrical Engineering
University Park, PA 16802

ABSTRACT

Gas proportional counter arrays based on the micro-well are an example of a new generation of detectors that exploit narrow anode-cathode gaps, rather than fine anodes, to create gas gain. These are inherently imaging pixel detectors that can be made very large for reasonable costs. Because of their intrinsic gain and room-temperature operation, they can be instrumented at very low power per unit area, making them valuable for a variety of space-flight applications where large-area X-ray imaging or particle tracking is required. We discuss micro-well detectors as focal plane imager for Lobster-ISS, a proposed soft X-ray all-sky monitor, and as electron trackers for the Next Generation High-Energy Gamma Ray mission.

We have developed a fabrication technique using a masked UV laser that allows us both to machine micro-wells in polymer substrates and to pattern metal electrodes. We have used this technique to fabricate detectors which image X-rays by simultaneously reading out orthogonal anode and cathode strips. We present imaging results from these detectors, as well as gain and energy resolution measurements that agree well with results from other groups.

Keywords: Micro-well, CAT, WELL, GEM, Avalanche, Gas detector, Proportional counter, Pixel detector, X-ray image

1. THE MICRO-WELL DETECTOR CONCEPT

We are developing pixel proportional counters based on arrays of micro-wells (or micro-well detectors) for large-area imaging for both X-ray and gamma-ray astronomy. Detectors based on the micro-well are one of a new, post-microstrip generation of gas proportional counters that exploit micro-machined, narrow-gap electrodes. Micro-well based detectors include the CAT[1,2], Micro-CAT[3,4], WELL[5], micro-well[6], and Micro-Wire[7]. This new generation of counters includes other geometries such as the Gas Electron Multiplier (GEM), MICROMEGA, and the Micro-Dot detector (see recent reviews[8,9]).

Each pixel of a micro-well detector consists of a charge-amplifying micro-well as shown in cross-section in Figure 1. The well itself is a cylindrical hole formed in an insulating substrate. The cathode is a metal annulus around the opening of the well. The anode is a metal pad at the bottom of the well. The sensitive volume is a gas-filled region between a planar drift electrode above the cathode and the micro-well.

With suitable voltages applied to the three electrodes, ionization electrons in the sensitive volume are drawn into the well toward the anode. In the well, the electric fields are strong enough to create an ionization avalanche. Electrons from the avalanche are collected at the anode, while an equal, but opposite, charge appears on the cathode.

An array of micro-well pixels forms a micro-well detector. Depending on the application, two-dimensional images may be obtained by reading out the anodes individually as pixels or by reading out the anodes connected in rows and the cathodes connected in columns to form an orthogonal crossed-strip coordinate system. Three-dimensional images of particle tracks could be derived with the addition of drift time measurements.

X-Ray and Gamma-Ray Instrumentation for Astronomy XI, Kathryn A. Flanagan, Oswald H. W. Siegmund,
Editors, Proceedings of SPIE Vol. 4140 (2000) © 2000 SPIE · 0277-786X/00/$15.00

Micro-well detectors have a number of distinct advantages for large area imaging, especially for space-flight applications. They offer a practical means of high-resolution (~100 micron) imaging over large areas at reasonable cost and power consumption.

Unlike traditional multi-wire proportional counters, the anodes and cathodes of micro-well detectors are rigidly affixed to a substrate. This greatly simplifies their construction and housing and allows much finer pitch. The micro-well electrodes can be formed using standard printed circuit techniques. Unlike micro-strips, the electrode metals can be wide and thick, making them able to withstand repeated breakdown without damage. Because these detectors require no special materials or handling, they are inexpensive to manufacture. The detectors we manufacture cost about one dollar per square centimeter in small quantities.

Due to their field geometry, micro-well detectors are highly stable, even at very high gas gains. Unlike micro-strip detectors, the avalanche region of a micro-well *is* the high-field region. Micro-well detectors routinely reach gas gains of 3 x 10^4. Also, since the avalanche occurs deep in the well, most UV photons from the avalanche are absorbed in the walls, naturally preventing breakdown from photon feedback and obviating the need for a quench gas. Micro-well detectors are stable in both pure Argon and pure Xenon, although with some sacrifice of energy resolution.

Micro-well detectors are naturally imaging. Not only are they imaging due to their pixel geometry, but anode and cathode collect equal signals, allowing simple crossed-strip imaging. Micro-well detectors are also a natural time expansion chamber, offering the possibility of three-dimensional imaging at reasonable power consumption. The drift fields and avalanche fields can be independently adjusted, allowing low drift fields and thus low drift velocities.

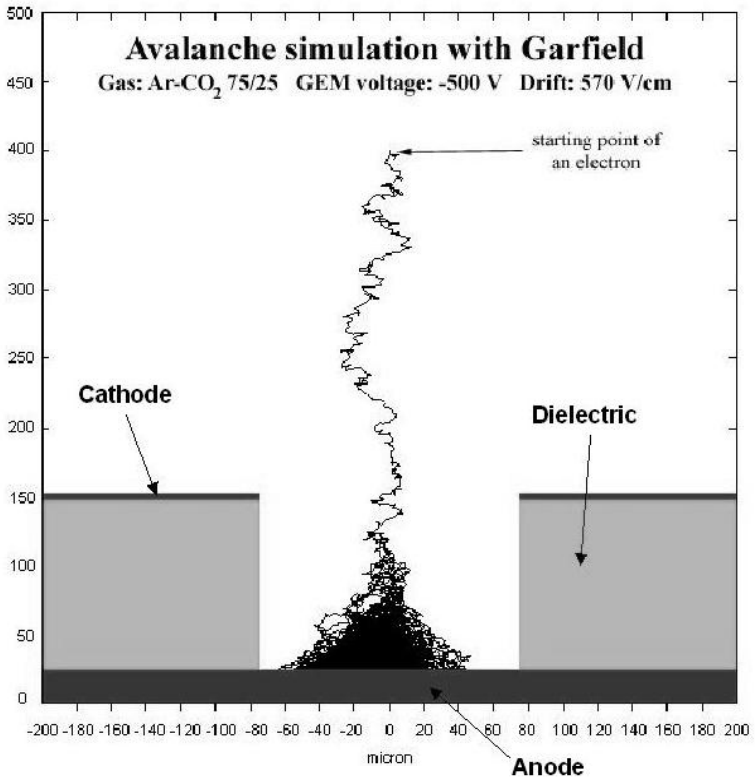

Figure 1. Cross section of a micro-well showing a simulated avalanche from a single primary electron.

2. APPLICATIONS IN HIGH-ENERGY ASTROPHYSICS

We are developing these detectors for two distinct kinds of applications, X-ray imaging and track imaging.

2.1 X-ray Imaging

Figure 2 illustrates "crossed-strip" segmentation for X-ray imaging, in which one coordinate of the avalanche is determined by reading out the anodes, and the other from reading the cathodes. We are developing this type of imager for the focal plane detector of Lobster-ISS[10], a soft X-ray all-sky monitor targeted for launch in 2005, which is currently the subject of an ESA accommodation study for the International Space Station.

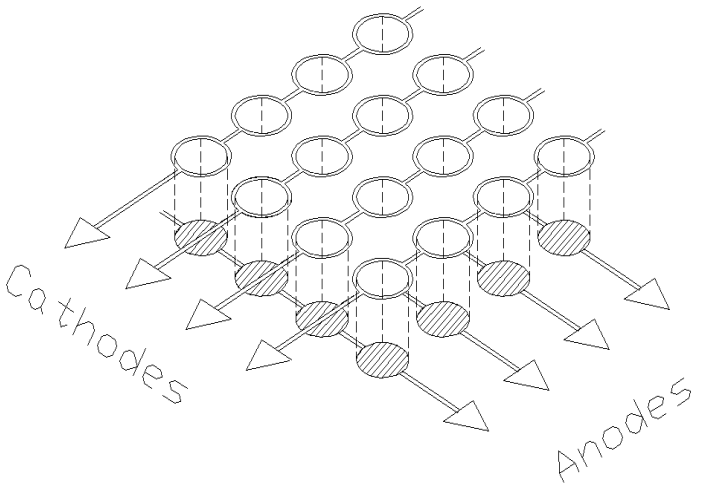

Figure 2. For X-ray imaging, the anode and cathode are both segmented.

Lobster-ISS requires six 20 x 20 cm^2 focal plane detectors, each with 250 μm imaging resolution and 0.2-3.5 keV bandpass. The cost and power requirements of tiling such a large area with CCDs are prohibitive, and therefore imaging gas detectors are required. Multi-wire or microstrip gas proportional counters might, in principle, be able to fulfill the Lobster requirements. Multi-wire counters, however, are mechanically complex, with multiple thin wire planes suspended under high tension. Micro-strip are unstable and fragile at high gain, and a rear cathode with inferior resolution is required for imaging. Considering these factors, well detectors are the logical choice.

Ideally, Lobster will fulfill its mission without a gas replenishment system. We are currently developing large-area X-ray windows with the goal of producing sufficiently low leak rates to obviate a replenishment system while fulfilling the band-pass requirement. The well detector's ability to operate with a pure Xenon gas fill simplifies the leak rate requirements on the window. If a multi-component gas is used, differences between leak rates will cause the gas composition, as well as the total pressure, to change with time.

2.2 Charged Particle Tracking

We are also developing electron trackers for the Next Generation High Energy Gamma-Ray Mission (NGHEG), a long-term mission recommended by NASA's Gamma-Ray Astrophysics Working Group (GRAPWG 99)[11]. The crossed-strip readout scheme has shortcoming for charged particle imaging applications, and we are therefore developing a separate segmentation and readout scheme for this application.

The principle limitation of the crossed-strip scheme is that to achieve reasonable three-dimensional imaging, only a small fraction of the track can be sampled in each detector, and many thin detectors are therefore required to accurately measure a track trajectory. An inclined charged particle passing through a crossed-strip detector geometry typically crosses several anode and cathode strips. The entrance and exit point of the track can be inferred from these independent x and y measurements, and the known positions of drift electrode and cathode. Trajectories are reconstructed by centroiding the hit strips. Position resolution in such a detector is limited by the pitch and by the mean distance between ionization events. If one wishes also to measure pairs of nearby inclined tracks individually (as is the case in a pair-production gamma-ray telescope), the x and y strips hit by each track must also be separated by at least one pitch unit. Thus the two-track resolution depends on the angle of inclination and the thickness of the detector's active region (the drift region in the case of well detectors). The drift region can be made thin to improve two-track resolution, but this reduces the signal and the sampled fraction of the track trajectory, as well as introducing the significant mechanical complication of suspending a drift electrode at a controlled distance (~1—3 mm) above the cathode.

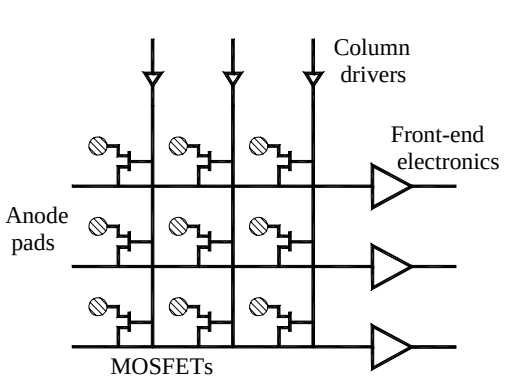

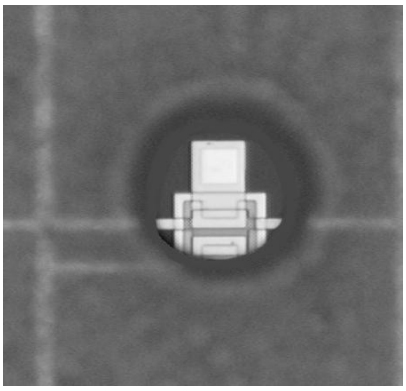

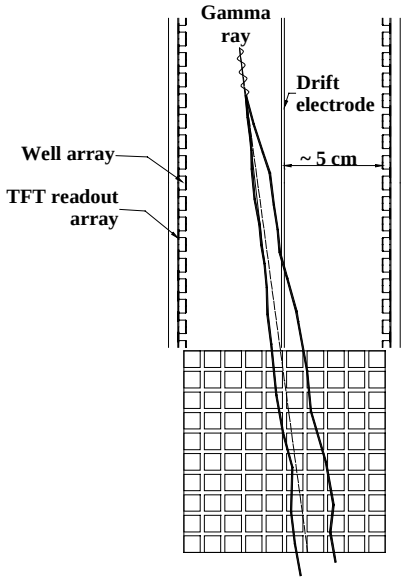

Figure 3. (Top left) Pixelized readout concept. (Bottom left) Lithographically fabricated well on top of a-Si:H thin-film transistor fabricated at Penn State. (Right) Stereo imaging concept for a very large area gamma-ray pair-production telescope.

One way to improve upon the tracking performance is to implement a time-projection chamber to provide true three-dimensional imaging. Since the third coordinate is inferred from drift time rather than the boundary of the active volume, the drift distance can be increased to many cm, drastically increasing the sampled fraction of the track trajectory. Well detectors are especially attractive for this application because they are natural time expansion chambers, that is, the avalanche field and drift field can be adjusted independently. This reduces the instrument's power requirements by allowing a slow drift speed simultaneously with a high gain. Nevertheless, power consumption is a major design issue for space instrumentation using this readout scheme. The lowest power TPC front end of which we are currently aware is the one for the Silicon Vertex Tracker on STAR, which consumes approximately 15 mW per channel.

Because the power consumption of a time expansion chamber is currently prohibitive for NGHEG, which will instrument many cubic meters, we are developing an extremely low-power readout system which sacrifices true three-dimensional imaging but still samples nearly the entire track. This is accomplished by storing charge on individual anode pixels until a trigger is received. Between readout cycles, the readout system operates in "sleep mode." The pixelized readout scheme is illustrated in Figure 3. Each anode pad is attached to a transistor. To read out a column, it is selected with a column driver, and the charge stored on each anode pad is collected at the front end of a charge integrating amplifier that serves each row. The charge in every individual row is thus measured, forming a two-dimensional projected image of the track. Because only the anode is read out in this scheme, the cathode can be used to generate a real-time trigger. In this sense the instrument can be self-triggering.

A "stereo" three-dimensional trajectory can be reconstructed without any timing information as the track passes through two or more detectors oriented in different directions (see Figure 3). Preliminary simulations indicate that a pair production gamma-ray telescope based on this concept would have single-photon pointing accuracy approaching the nuclear recoil limit up to 1 GeV, and achieving 1 arcmin at 10 GeV. There is not a hard dividing line between the time expansion chamber approach and the pixelized charge storage approach; performance of the stereo imager could be improved even further by sparsely populating the detectors with timing channels.

We are currently developing amorphous hydrogenated silicon (a-Si:H) arrays of thin-film transistors with the goal of demonstrating a small stereo tracker. The a-Si:H readout technology has already been implemented in several commercial large-area X-ray imagers for medical and industrial applications[12].

3. UV LASER MACHINING

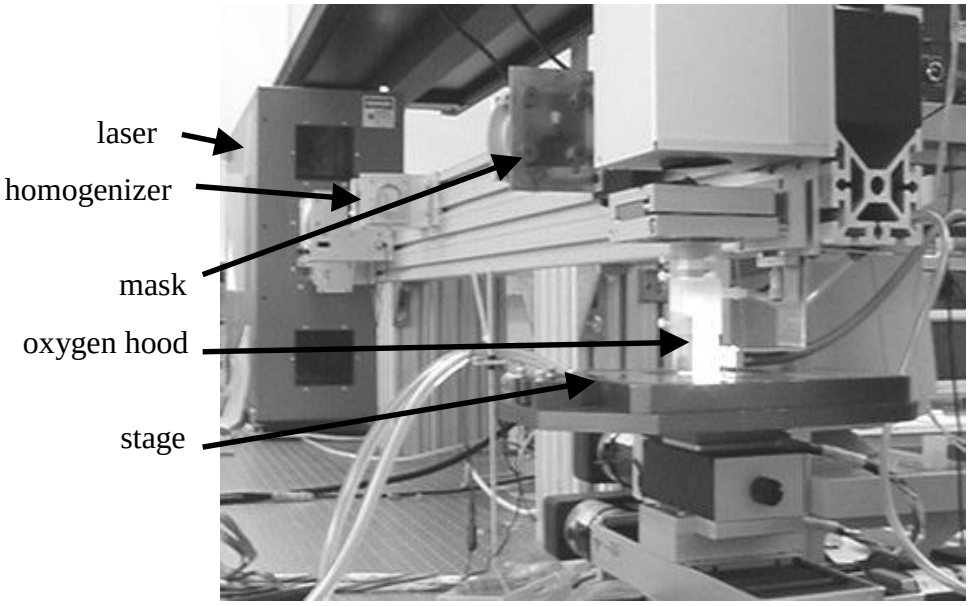

Figure 4. UV laser beam line and stage at Goddard Space Flight Center

Micro-well detectors or similar detectors have been fabricated using solid metal cathodes suspended over an anode substrate[1-4], etching[5,7], and UV laser ablation[6]. Electro-formed cathodes minimize the amount of dielectric in the detector, but are difficult to produce in large area, and furthermore cannot easily be segmented, since these detectors have no supporting substrate. Etching is probably the fastest and therefore least expensive method for fabricating large detectors. UV ablation allows the finest and most flexible control of the machining process, and has the additional benefit that it can be used to finely pattern thin (<1 μm) metal. However, we have had to develop special techniques to excavate the without leaving carbon buildup on the sides of the wells.

The laser ablation technique takes advantage of the fact that most polymers are ablated by intense UV light, but metal thicker than a few μm acts as a stop layer. We ablate the polymer substrate using our masked 248 nm UV laser facility (Figure 4) to form the wells in the polymer substrate. The pulsed beam is homogenized, passed through a shadow mask, and demagnified by a factor adjustable from 4.8 to 5.4. The demagnified mask image illuminates an 2.5 x 2.5 mm^2 square on the detector, which is affixed to a vacuum chuck stage with 20 x 20 cm^2 travel. The shape of the openings in the mask and motion of the stage during the ablation process controls the shape of the wells. A CCD camera mounted behind a partially reflecting mirror allows real time viewing of the region being machined.

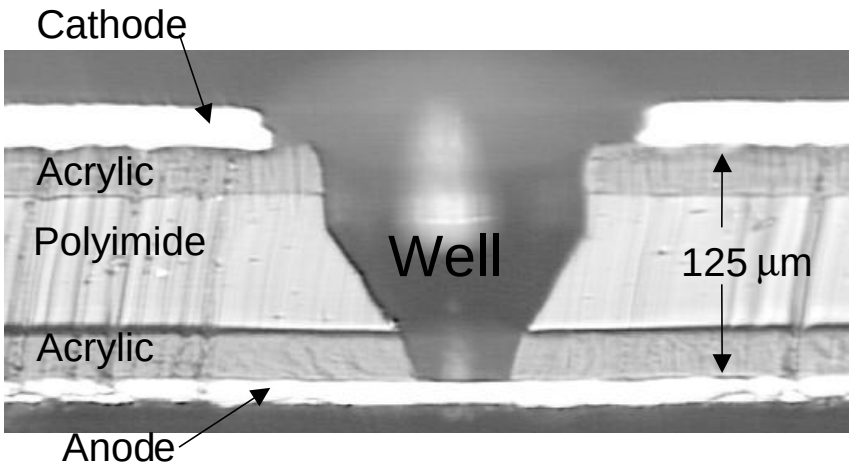

Figure 5. Cross-section of a well with commercially fabricated cathode and anode. The funnel-like shape of the well is made by machining with an undersize mask while executing a circular motion with the stage.

The detectors discussed in this paper were fabricated on commercially available flexible dielectric substrates consisting of 1 mil of acrylic cladding around a polyimide core (Figure 5). The anodes were commercially etched from half-ounce (18 μm) copper cladding on the substrate. The cathodes were also etched, but 500 Å platinum was also sputtered on top of the

segmented cathodes of the imaging detectors prior to machining the wells. The platinum is then patterned with the laser, yielding thinner isolation cuts than are possible with commercial etching (Figure 6). For most of the imaging detectors, the platinum within the circular copper void was also removed, leaving a 200 μm void, but in one detector, the platinum was not removed, resulting in voids of 125 μm, the same diameter as the mouth of the wells. Platinum was not deposited on the non-imaging, solid-cathode detectors.

3.1 Machining Techniques

We have identified several kinds of manufacturing defects present in detectors that break down at low voltage, that is, a voltage corresponding to a gas gain below 20,000-30,000. Detectors usually either achieve gains of at least 20,000 at ~650 V in 600 Torr P-10, or they break down or draw current at ~200 V below this. It is usually possible to identify individual wells that have broken down, either by observing discoloration of the cathode after the fact, or by directly observing the spark in a transparent flow box.

We list three manufacturing defects, and the machining techniques we employ to prevent them, below.

Carbon deposits. When present on the walls of the wells, these deposits can cause low-voltage breakdown. To prevent this buildup, we combine three techniques. First, the ablation is performed in a flowed oxygen atmosphere to promote full combustion of ablation byproducts. Second, the wells are milled while the stages are executing a circular motion (typically with 12 μm radius, but this value is not critical) so that material deposited on the walls is continuously ablated away, exposing fresh polymer. Finally, the detector is put in a weak detergent ultrasound bath for 3-5 minutes. The detergent reduces surface tension to allow the solution to more readily enter the wells. Although we have successfully fabricated detectors without implementing all of these measures, we have found that a high yield requires all three.

Exposed Cathode Rims. When machining detectors with commercially etched cathodes, we have found it to be necessary to leave a thin dielectric annulus inside the cathode void, as shown in Figure 6. Failure to leave a complete annulus around even a small fraction of the wells invariably results in low-voltage breakdown. The reason for this failure mode is unclear. Either the laser damages the etched cathodes, or some quality of the etched metal, such as surface roughness, is responsible the breakdown. However, we note that cathodes constructed using other methods do not require this annulus. We have built and operated detectors in which the substrate and cathode are made with the same materials by the same manufacturer, but in which the wells are mechanically drilled. Some of these wells had metal at their rims, but these detectors nevertheless reached gains of ~30,000. We are currently fabricating and testing sputtered cathodes, and results from one such detector indicate that sputtered cathodes do not require this annulus. Other groups have also reported results from detectors without this dielectric annulus.

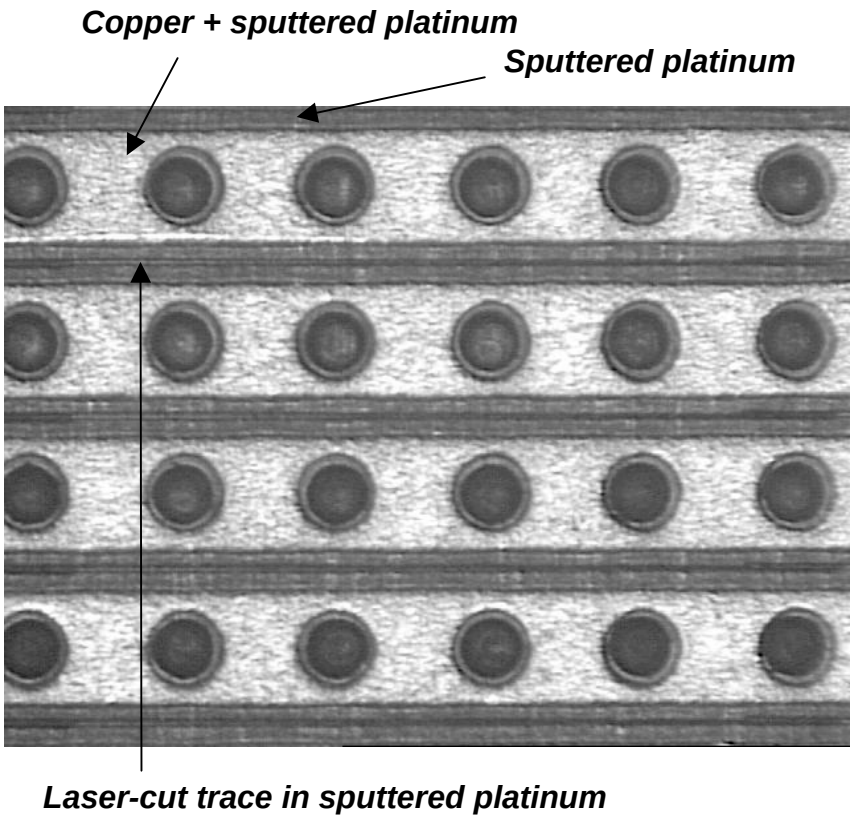

Figure 6. Portion of a well array which has been sputtered with platinum prior to machining. Thin isolation traces were cut in the platinum, and the platinum inside the copper voids removed.

We have written stage and laser control software to automatically align the

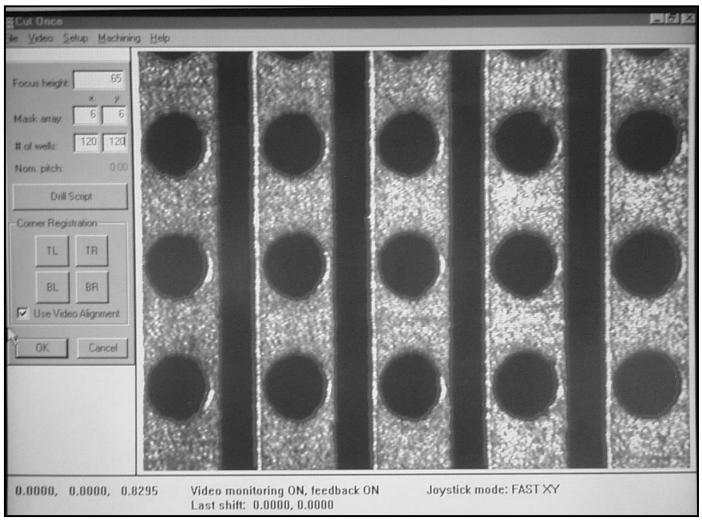

Figure 7. Screen shot from control software, which integrates laser control, stage motion, and automatic image-analysis driven registration.

masked laser pattern with pre-manufactured anodes and cathodes to the required accuracy (Figure 7). To use the software, a high-contrast CCD image of the mask pattern is first produced by ablating an aluminized mylar film. The edges of the resulting pattern are detected, stored, and displayed as an overlay on the live camera image. The user manually centers the mask pattern on a region of the cathode (at this time, stage rotation and beam demagnification are checked and adjusted if necessary) and an image of the cathode is edge-detected and stored. This image is later used by the software as a template to fine-tune alignment during machining. The user inputs information specifying the size, position, and pitch of the array to be machined, and specifies a file that contains specific instructions to the laser and stage to be executed at each step-and-repeat iteration. Machining is then begun. At each step, the software detects the edges of the cathode pattern currently being displayed, compares it to the cathode template, and adjusts the stage position to maximize overlap before machining. The centering accuracy of this system is typically better than 10 μm, limited by variations in the cathode shape.

Exposed Anode Edge. We have observed low-voltage breakdown in detectors in wells in which the edge of the anode pad is barely exposed, which can occur when the anode and cathode are not aligned. Low-voltage breakdown does not seem to occur in wells in which the anode edge is completely covered by dielectric, or in wells where the anode edge is separated from the dielectric by more than a few μm. We avoid this manufacturing defect by intentionally isolating the anode pad from the dielectric by removing about 10 μm of dielectric around the edge of the anode pad.

4. MICRO-WELL DETECTOR PERFORMANCE

Measurements of detector performance have been made with 5 cm x 5 cm detectors with 400 micron pitch machined at Goddard as described in section 3. The parameters of primary interest are position resolution, gas gain, and energy resolution. The test setup is shown in Figure 8. Measurements were made in vacuum system equipped with a bell jar at slightly less than one atmosphere. Gas was not flowed through the system.

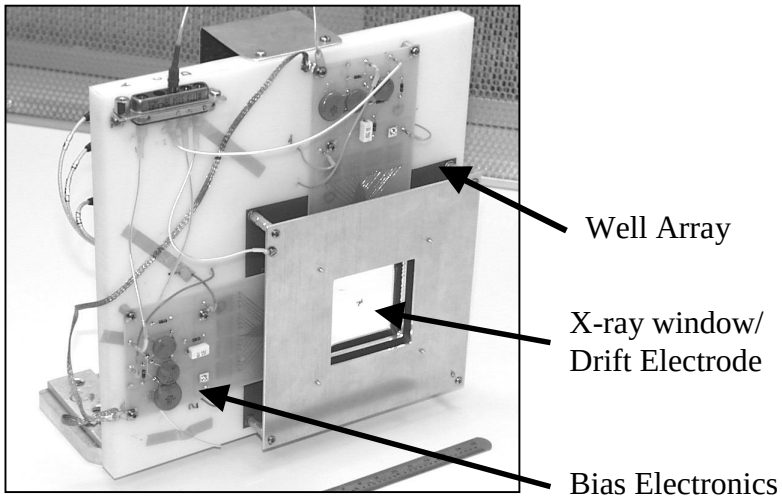

Figure 8. 5-cm detector in test stand ready to be mounted in vacuum system. Four charge preamplifiers are mounted on the reverse side of the test stand (not visible in the photograph).

4.1 Gas Gain

Gas gain measurements were made for detectors of various widths and at different pressures of P-10 (90% Argon, 10% Methane). The measurements were made collecting pulse-height spectra of X-rays from an ^{55}Fe source. The peak of

the spectrum was compared to the pulse height from a known charge injected into the electronics. The gain was then calculated assuming 230 primary electrons created in Argon from the 5.9 keV photons. It is possible for all the primary electrons not to be collected (see section 4.3), thus causing the gain to be underestimated. However, the gain measurements were made in detectors that had high collection efficiency.

Typical gas gain curves up to the limit of stability are shown in Figure 9 for detectors of different thickness. In all cases, the detectors had 400 μm pitch and 200 μm circular voids in otherwise solid cathodes. The slope of these curves is steeper than for wire proportional counters and is consistent with other published measurements[1-6]. There is some evidence that thicker detectors are more stable, but we have not investigated this carefully.

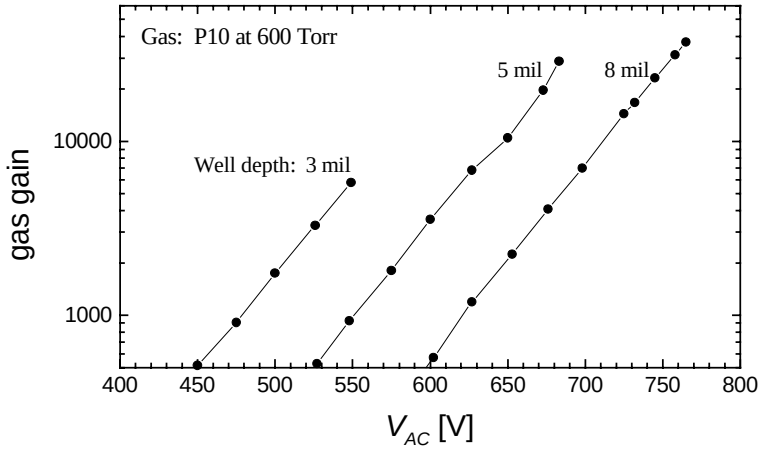

Figure 9. Gain curves for several thickness of substrate. The electrode layouts are identical in each case.

We have also found that the gain behavior is remarkably insensitive to the shape of the anode. We have investigated the gain for detectors with different anode sizes and shapes, including round pads of different sizes and simple strips of different sizes that ran through the bottom of the well. No significant variation in the gain curve was ever observed. This is consistent with other observations[2,13] that the avalanche occurs on the axis of the well, as all anode geometries had metal at the center of the well.

4.2 Image Resolution

Position resolution in two dimensions was measured over a 12.4 mm x 12.4 mm region of crossed-strip anodes and segmented cathodes strips as described in section 2.1. Position encoding was done by charge division in each dimension by connecting the metal electrode strips to a resistor chain. The anodes were connected together in a resistor chain with 2 kΩ between adjacent anode strips. Each end of the chain was connected to a charge sensitive amplifier, shaping amplifier, and sample and hold circuit. The cathodes were similarly connected. The four signal amplitudes were digitized and the positions calculated as:

$$X = \frac{Q_{anode1}}{Q_{anode1} + Q_{anode2}} \text{ and } Y = \frac{Q_{cathode1}}{Q_{cathode1} + Q_{cathode2}}.$$

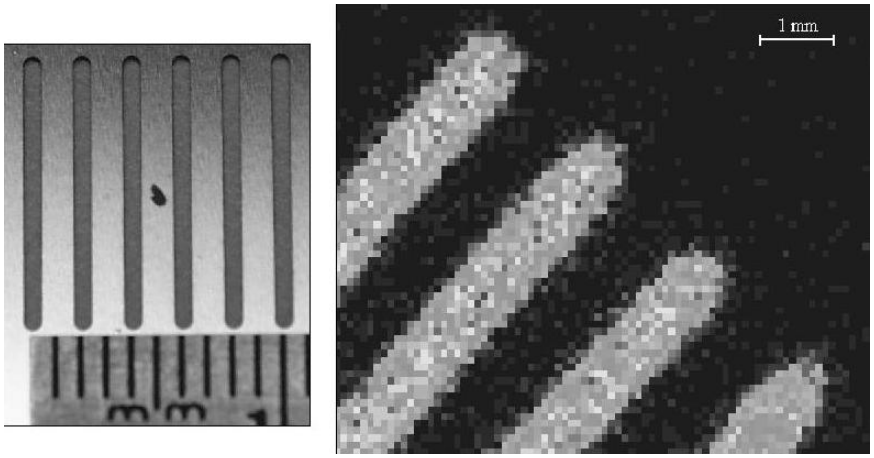

Figure 10. Image (right) of slotted stainless steel shadow mask (left). The mask has 750 μm slots on a 2mm pitch.

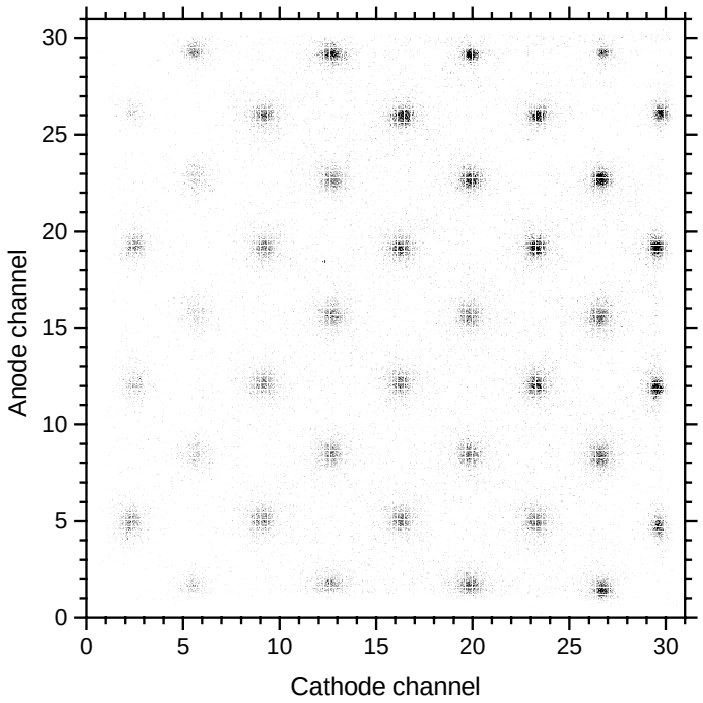

Figure 11. X-ray image of a pinhole array taken with a crossed-strip detector. The pinholes are on a 2 mm pitch.

Figure 10 shows the image of shadow mask illuminated by ^{55}Fe X-rays. The image clearly demonstrates that the cathodes and anodes provide equal position resolution, which is about 300 microns FWHM in each dimension.

Position resolution measurements were made by illuminating a pinhole shadow mask with an X-ray tube arranged to minimize parallax effects. Figure 11 shows the image of a shadow mask that is an array of 75 μm pinholes on a 2 mm pitch. This mask was illuminated with the 2-10 keV bremsstrahlung spectrum from an X-ray tube about 120 cm from the detector. The drift depth was about 3 mm.

Contributions from the noise in the encoding are less than 100 μm for all energies. If the pinhole images arise from a single hit well, we would therefore expect 100 μm spots on a discrete grid corresponding to the pitch of the well array, with the error dominated by the binning error which is equal to the pitch/√12. Instead, we see 300 μm spots and no evidence of pixelization. Thus we conclude that the individual X-ray images are generated by a centroid over several pixels of the diffused photo-electron cloud. Presumably, the measurement error is due to statistical fluctuations in the individual wells (fluctuations in both the incident number of photo-electrons and the subsequent avalanche sizes), but we have not modeled this in detail.

4.3 Energy Resolution

Fractional energy resolution (ΔE/E) in a proportional counter is inversely proportional to the square root of the number of primary electrons that create the avalanche. As in any proportional counter, primary electrons may be lost to recombination in the drift region, especially at low drift fields.

In the micro-well detector, additional losses may occur if the geometry is such that drift field lines terminate on the cathode (or on a dielectric surface). If the spacing between wells is too large, or the depth of the well too great, or both, primary electrons will be collected on the cathode. This causes a loss of resolution that is enhanced at higher drift fields[4]. Another possible loss mechanism for detectors with segmented cathodes is electrons being drawn to the anode connection traces through the gaps between the cathode strips, thus being lost on the dielectric.

Figure 12 shows the spectrum from a micro-well detector that exhibits 20% FWHM energy resolution for 5.9keV X-rays in P-10. This detector was 125 μm thick with 200 μm diameter cathode voids on a 400 μm pitch. This is close to the theoretical best resolution for a gas proportional counter in Argon. Also, the gain and energy resolution were virtually insensitive to the strength of the drift field.

Detectors with even slightly smaller void sizes, however, displayed behavior consistent with loss of primary electrons at the cathode. Similar detectors with voids of 175 μm and 125 μm diameter showed a loss of both signal and resolution at all but very low drift fields.

The energy resolution of detectors with segmented cathodes has also been investigated. Loss of resolution for detectors with 100 μm separation traces between cathode strips was found to be severe. However, no noticeable loss of resolution was observed with the approximately 15 μm laser-machined separation traces.

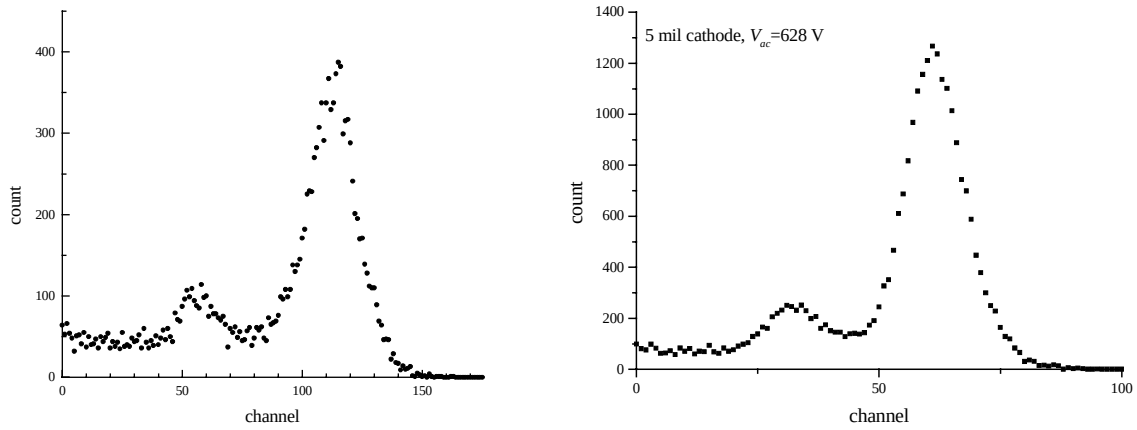

Figure 12. (Right) Fe-55 spectrum from detector with 200 μm cathode voids. This cathode was not segmented into strips. (Left) Fe-55 spectrum from detector with 125 μm cathode voids and segmented cathode strips. The drift field was approximately 100 V/cm, and the drift distance was one cm. At higher drift fields, the signal size and energy resolution in this small-void detector decrease. The anode-cathode voltage was 550 V for the spectrum on the right, giving a gain similar to the gain to the gain on the left, approximately 8000.

5. FUTURE WORK

Future work will include instrumenting the detectors on an amplifier per electrode basis. While charge division may prove adequate for our intended uses, an amplifier per electrode readout will allow us to study the shape of the charge clouds. Lifetime testing of the well detectors in noble gases and mixtures is necessary to qualify well detectors for space applications. Refining our detector geometry and machining techniques may increase yield and charge collection efficiency. Integrating thin film transistors onto the well detector array, while straightforward in principle, needs to be demonstrated. The Lobster-ISS detectors require integrating well detectors with thin, low leakage windows.

REFERENCES

[1] F. Bartol, M. Bordessoule, G. Chaplier, M. Lomonnier and S. Megtert, "The C.A.T. Pixel Gas Counter Detector," *J. Phys. III France* 347, pp. 337-347, 1996.

[2] G. Chaplier, J.P. Boeuf, C. Bouillot, M. Lemonnier, S. Megtert, "Prelimary results of the experimental and simulated instrinic properties fo the Compteur A Trou (CAT) detector: behavior with synchrotron radiation," *Nucl. Instr. and Meth. A* 426, pp. 339-355, 1999.

[3] A. Savestani, H.J. Besch, M. Junk, W. Meiβner, N. Pavel, N. Sauer, R. Stiehler, A.H. Walenta, R.H. Menk, "Gas amplifying hole structures with resistive position encoding: a new concept for a high rate imaging pixel detector," *Nucl. Instr. and Meth. A* 419, pp 444-451, 1998.

[4] A. Savestani, H.J. Besch, M. Junk, W. Meiβner, N. Sauer, R. Stiehler, A.H. Walenta, R.H. Menk, "Study and application of hole structures as gas gain devices for two dimensional high rate X-ray detectors," *Nucl. Instr. and Meth. A* 410, pp 238-258, 1998.

[5] R. Bellazzini, M. Bozzo, A. Brez, G. Gariano, L. Latronico, N. Lumb, A. Papanestis, G. Spandre, M.M. Massai, R. Raffo, M.A. Spezziga, " The WELL detector," *Nucl. Instr. and Meth. A* 423, pp 125-134, 1999.

[6] P. Deines-Jones, J.K. Black, H. Crawford, S.D. Hunter, "Imaging Micro-Well Proportional Counters Fabricated with Masked UV Laser Ablation," to be published, Nucl. Inst. and Meth. A.

[7] B. Adeva, F. Gomez, A. Pazos, R. Pfau, M. Plo, J.M. Rodriquez, P. Vazquez, J.C. Labbe, "The Micro Wire Detector," *Nucl. Instr. and Meth. A* 435, pp 402-407, 1999.

[8] Fabio Sauli, "Gas detectors: Recent developments and future perspectives," *Nucl. Instr. and Meth. A* 419, pp 189-201, 1998.

[9] Fabio Sauli, "Recent developments and applications of fast position-sensitive gas detectors," *Nucl. Instr. and Meth. A* 422, pp 257-262, 1999.

[10] Fraser, G.W., *et al.*, "An Imaging All-Sky Monitor based on Lobster Eye X-ray Optics. An International Space Station (ISS) Attached Payload submitted in response to the ESA Call for Mission Proposals for the Flexi-Missions F2 and F3", submitted to ESA, January 2000.

[11] Gamma-Ray Astronomy Programs Working Group (GRAPWG), "Updated Science Priorities: February 1999, NP-1999-04-072-GSFC, available at http://universe.gsfc.nasa.gov/grapwg/grapwg_brief.pdf , 1999.

[12] L.E. Antonuk,Y. El-Mohri, A. Hall, K.-W. Jee, M. Maolinbay, S.C. Nassif, X. Rong, J. J. Siewerdsen, Q. Zhao, "Large-area 97-mm pitch indirect-detection active-matrix flat-panel imager (AMFPI)," Proc. of SPIE, 3336, pp. 2-13, 1998.

[13] G. Chaplier, M. Lemmonnier, S. Megtert, "Derivation of a simple analytical expression of the gain of pure argon filled CAT porportional counters," *Nucl. Instr. and Meth. A* 440, pp 466-470, 2000.